Satellite observations of plasma physics near the magnetic field reconnection X line

F. S. Mozer,[1] D. Sundkvist,[1] J. P. McFadden,[1] P. L. Pritchett,[2] and I. Roth[1]

Received 25 August 2011; revised 15 October 2011; accepted 17 October 2011; published 21 December 2011.

[1] Satellite observations near the X line are required to understand electromagnetic energy conversion and particle acceleration resulting from magnetic field reconnection. More than 900 orbits of Time History of Events and Macroscale Interactions during Substorms (THEMIS) spacecraft across the low-latitude dayside magnetopause, involving more than 4000 magnetopause crossings and 5000 h of data, were searched for examples of magnetic field reconnection within a few electron skin depths of the X line. Evidence that the X line was crossed in the best of these events comes from observations of DC electric and magnetic fields, electrostatic and electromagnetic lower hybrid waves, magnetosheath electrons flowing along the separatricies, and a super-Alfvenic electron jet flowing perpendicular to the magnetic field. A dispersion analysis identifies properties of the wave that are in agreement with the experiment. Neither these waves nor the DC electric field were sufficient to account for acceleration of the electron jet. The anomalous drag was not an important source of the observed DC electric field. The observed pressure gradient is a possible candidate for maintaining the electric field.

Citation: Mozer, F. S., D. Sundkvist, J. P. McFadden, P. L. Pritchett, and I. Roth (2011), Satellite observations of plasma physics near the magnetic field reconnection X line, *J. Geophys. Res.*, *116*, A12224, doi:10.1029/2011JA017109.

1. Introduction

[2] Magnetic field reconnection is generally thought to be the mechanism responsible for triggering rapid conversion of electromagnetic energy to plasma energy, leading to the acceleration of energetic particles in Earth's magnetosphere, solar flares, and astrophysical objects. To understand reconnection, it is necessary to measure and understand the fields and plasmas at the reconnection site, which is the location where magnetic fields from two different topologies meet and reconnect near an X line. Toward this goal, 900 orbits of THEMIS satellites that passed across the dayside magnetopause in 2009 and 2010 and that encountered some 4000 dayside magnetopause crossings were searched for events occurring near the X line. If these satellite crossings occurred randomly over a distance of 50 ion skin depths (2000 electron skin depths) from the X line, the chances that a few events occurred within one or a few electron skin depths from the X line would be good. A major component of this search involved monitoring the 1 keV electron flux, which is expected to be enhanced by electron acceleration in the vicinity of the X line.

[3] Summary properties of the candidate with the largest flux of one keV electrons in these 900 orbits are given in Figure 1. The one keV electron flux in this event exceeded that of the second largest flux observed in the 900 crossings by more than a factor of two. Figure 1a gives B_Z, the reconnecting component of the magnetic field, during a 1 h interval including the event of interest. There were three magnetopause crossings during this hour, as signified by the changes in B_Z from positive to negative or vice versa. In the magnetosphere, where B_Z was positive, high-energy ions (Figure 1c) and electrons (Figure 1d) were encountered, while in the magnetosheath, lower-energy ions and electrons were measured. The flux of one keV electrons is plotted in Figure 1e. During the first two crossings, the largest one keV fluxes were in the magnetosphere and they decreased as the spacecraft passed from the magnetosphere to the magnetosheath. By contrast, the one keV electron flux observed at the magnetopause during the third crossing was an order of magnitude larger than at any other time during the hour of interest. Because this large flux did not exist in the magnetosphere or in the magnetosheath, these electrons must have resulted from local acceleration. In Figure 1b it is noted that the electric field was greater than 100 mV/m at the time of interest, which makes it a candidate for the acceleration of these particles. In section 2 it will be shown that the satellite passed through the X line within a few electron skin depths at the time of interest, and the properties of the particles and fields at this time will be examined.

2. Evidence of an X Line Crossing

[4] Figure 2 presents an overview of the magnetopause crossing of interest, which occurred at a geocentric altitude of 9.4 Earth radii, a local time of 12:38, and latitude of −10°. The data are presented in the minimum variance of B

[1]Space Sciences Laboratory, University of California, Berkeley, California, USA.
[2]Department of Physics and Astronomy, University of California, Los Angeles, California, USA.

0148-0227/11/2011JA017109

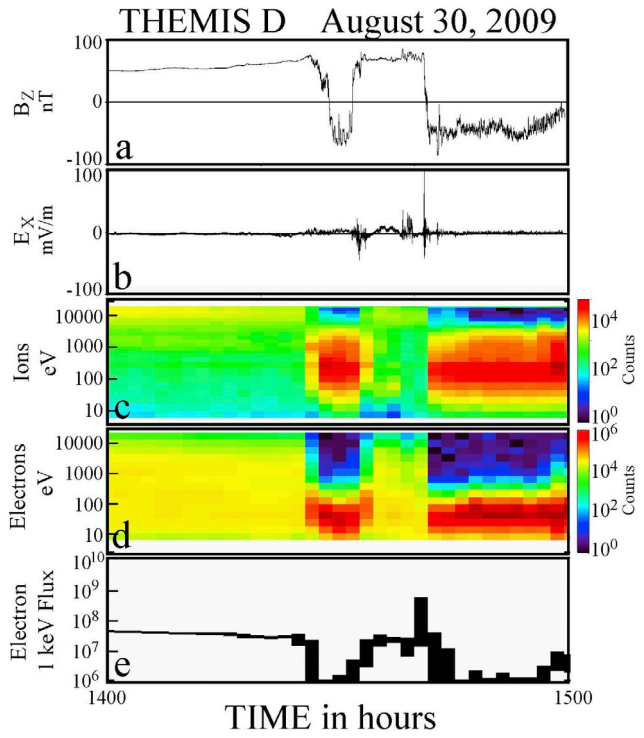

Figure 1. Fields and plasmas during a 1 hour interval involving three subsolar magnetopause crossings. The field data are presented in de-spun spacecraft coordinates which are close to GSE or minimum variance coordinates for this subsolar crossing.

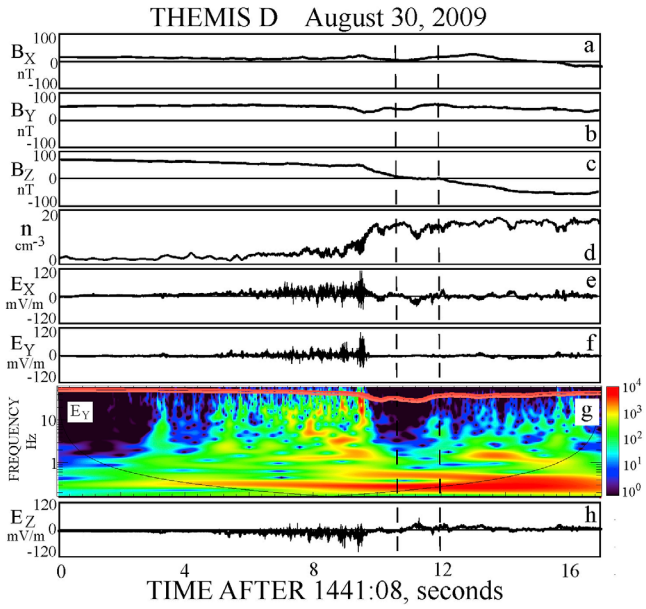

Figure 2. Electric and magnetic fields during the 17 s interval of a subsolar magnetopause crossing. The plasma density is inferred from the spacecraft potential.

coordinate system whose X direction is normal to the current sheet and points Sunward, while the reconnection magnetic field is in the Z direction pointing generally perpendicular to the ecliptic plane. That the spacecraft passed from the low plasma density magnetosphere to the higher-density magnetosheath during the 17 s interval of Figure 2 is shown by the factor of 10 increase of the plasma density in Figure 2d and, also, by the change of the reconnection magnetic field in Figure 2c from the positive value associated with Earth's dipole field to the negative value from the solar wind. During this crossing the electron beta was less than 0.02 everywhere because the guide magnetic field in Figure 2b (the ratio of the out-of-plane field to the reconnecting field) was 0.6. This field is much stronger than the typical value of 0.1 needed to magnetize electrons (having a 0.5 km radius of curvature) in the vicinity of the X line [*Swisdak et al.*, 2005]. The 3 s averaged ion and electron temperatures were isotropic within 15%, and they were 800 and 100 eV, respectively. Even though the absolute values of B_Z in the asymptotic regions were similar during this crossing, it involved asymmetric reconnection because of the large density ratio.

[5] Figure 3 gives data from a particle-in-cell simulation of subsolar 2-D, driven, asymmetric magnetic field reconnection with a guide field of 0.5 (computed as B_Y divided by the average of the absolute values of the sheath and sphere B_Z values), open boundaries, and an ion to electron mass ratio of 200 [*Pritchett and Mozer*, 2009a]. These data serve as a guide to the features expected near the X line which is at the center of the reconnection geometry inside the square box in Figure 3. In Figure 3 the magnetosphere is shown at right, and the black magnetic field lines are from the dipole-like magnetic field of Earth and they point upward; that is,

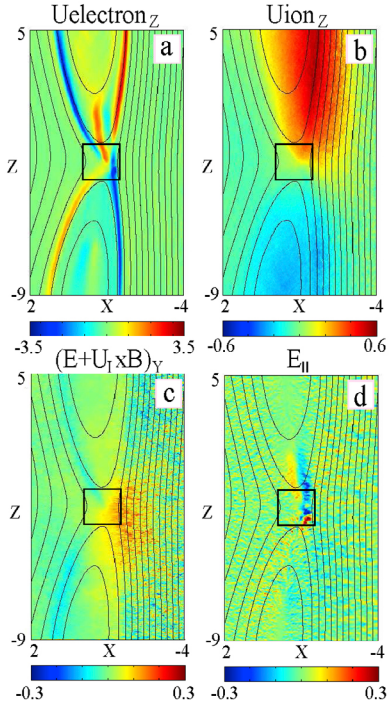

Figure 3. Simulations of the flows and fields near the X line of an asymmetric magnetopause crossing. The magnetosphere with its upward directed magnetic field lines is shown at right, and the magnetosheath with its downward magnetic field lines is shown at left.

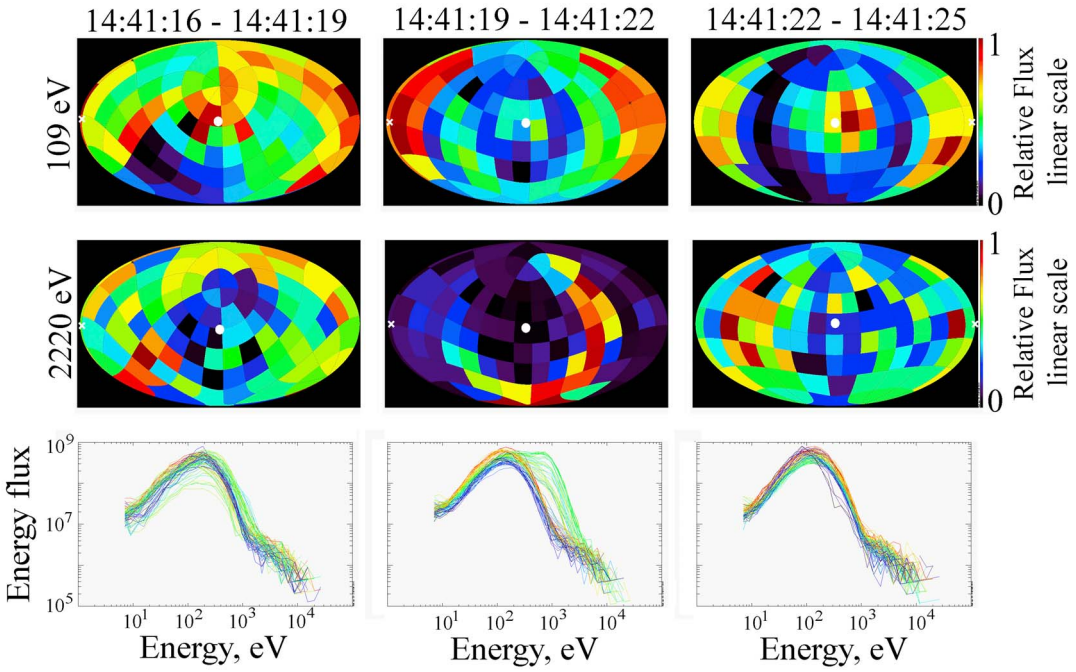

Figure 4. Electron fluxes and spectra at two energies during three successive three second satellite spin periods.

in the +Z direction. The magnetic field lines shown at left are in the magnetosheath and come from the solar magnetic field. They point in the −Z direction and this field is a factor of three smaller than the magnetospheric magnetic field. To satisfy curl**B** = μ_o**j**, where **j** is the current density, there is a current flowing out of the plane of Figure 3, in the +Y direction. This simulation provides information on what should be seen by a satellite passing near the X line. The data of Figures 2 and 3 are next compared.

[6] 1. Reconnection must occur for there to be an X line. This requires that $B_X \neq 0$, because this component is required for the magnetic field lines on the two sides to be connected. That B_X is nonzero in the simulation geometry of Figure 3 is seen from the field lines drawn. In Figure 2a, B_X is measured to be nonzero. Its positive value indicates that the satellite passed below the X line and this conclusion will be tested against other determinations of the satellite trajectory.

[7] 2. $B_Z \sim 0$ near the X line. This can be seen in Figure 3 inside the boxes. In Figure 2c, $B_Z \sim 0$ inside the two vertical dashed lines which is where the X line was crossed. During this period, B_Z changed by about 1 nT around its mean value of ∼0.

[8] 3. Field-aligned magnetosheath electron macroscopic flows along the magnetosheath separatrices (the approximate boundaries of the current sheet) are toward the X line and the flow is away from the X line along the magnetospheric separatrices. (In this and all further discussion, the flows refer to macroscopic flows as measured by a particle detector, and not to individual electron trajectories.) The Z component of the simulation flows of Figure 3a include magnetosheath electrons flowing parallel to B into the X line from the magnetosheath side and away from the X line on the magnetospheric side. Figure 4 shows the same electron flow in the experimental data. In Figure 4 the columns correspond to data collected during successive 3 s spin periods while the top two rows give the relative electron energy fluxes at 109 and 2220 eV, respectively. The magnetic field direction is at the center of each ellipse and the direction opposite to **B** is at the left and right peripheries. Thus, electron flows at a 0° pitch angle are at the center of a plot and flows at a pitch angle of 180° are at the periphery, while a 90° pitch angle flow forms a circle around the center of the ellipse. Consider the top row of electron fluxes at 109 eV. During the first 3 s period (which is before and up to the first vertical dashed line in Figure 2), the flows were distributed rather randomly in pitch angle while, during the second spin period (which comprises both the region where $B_Z = 0$ between the dashed lines in Figure 2 and time after the dashed lines), the flows were field aligned because the periphery of the ellipse is red, indicating that the largest flows were at a pitch angle of 180°. During the third spin period, there were counter-streaming field-aligned flows for a fraction of the time. Thus, for a time the order of 1 s, there were anti-field-aligned flows of magnetosheath electrons followed by a shorter duration of counter-streaming field-aligned flows, as expected from the simulation data. Because the main field-aligned flow was in the antiparallel direction, the spacecraft crossing must have been below the X line (see Figure 3a), in agreement with the sign of B_X discussed earlier.

[9] 4. Super-Alfvenic energetic electrons flow perpendicular to the magnetic field, away from the X line. This flow is seen in Figure 3a as the red trace extending upward from the X line, perpendicular to **B**. The experimental flows at 2220 eV in the second row of Figure 4 also display this feature. During the first and third spin periods the flows were rather random in pitch angle while, during the middle spin period, the outflow at 2220 eV was at a pitch angle near 90° for about half the spin period because the largest

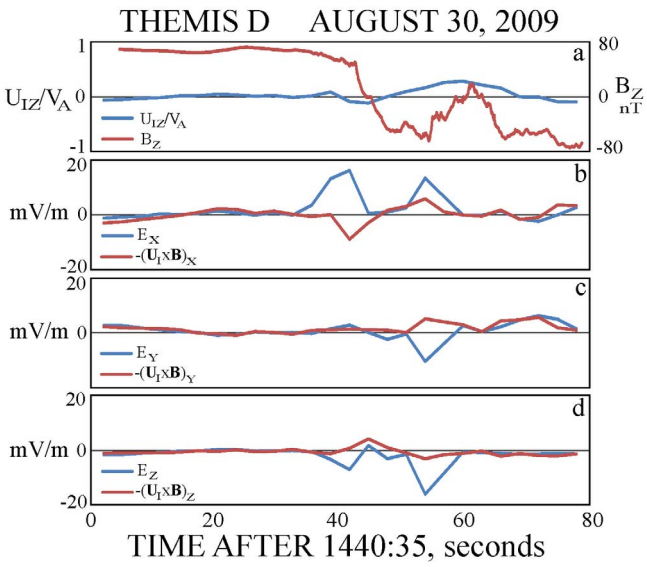

Figure 5. Spin period averaged flows and fields at the magnetopause crossing of interest. The statistical uncertainty in the speed ratio of Figure 5a is a few percent, which may be smaller than the uncertainty associated with time aliasing over the 3 s spin period.

fluxes formed a semicircle about the center of the ellipse. (If the flow lasted the entire spin period, the 90° fluxes would have formed a closed circle.) These features are also illustrated in Figure 4 in the bottom row of electron spectra at different pitch angles, with the blue and red spectra corresponding to flows at 0° and 180° respectively, while the green spectra correspond to pitch angles near 90°. In the central column, the near-90° fluxes above about 300 eV are enhanced by as much as two orders of magnitude relative to earlier or later times and the lower-energy 180° fluxes (the red curves) are enhanced over the 0° fluxes by a factor greater than three. The ~2 keV electrons are super-Alfvenic because their 30,000 km/s speed is about 2.5 times the electron Alfven speed in the magnetosheath. The pitch angle of the super-Alfvenic electron flow was centered at 90° and measured to have a full width at half maximum of less than 20° (not shown). It is noted that the perpendicular electron flow in the simulation of Figure 3a is at the local $\mathbf{E} \times \mathbf{B}/B^2$ velocity.

[10] 5. To be near the X line, the field-aligned low-energy electrons and the super-Alfvenic perpendicular electrons must be observed at the same time. The super-Alfvenic perpendicular electron jet and the field-aligned magnetosheath electron flow occur at the same time in the experimental data, to within a fraction of a second. The simulation of Figure 3a shows that these features occur near simultaneously only near the X line. Further from the X line, both flows would appear in a satellite crossing but they would be separated in time by an amount comparable to the crossing time.

[11] In the simulation, the super-Alfvenic jet occurs above the X line and the guide magnetic field is negative. In the satellite data, because the guide field of Figure 2b is positive, the super-Alfvenic outflow should be observed only below the X line. The actual observation of this flow indicates that the satellite passed below the X line, in agreement with the same conclusion reached from the sign of B_X and the sign of the field-aligned low-energy flow. The existence of a super-Alfvenic electron jets flowing out from the X line has been inferred from earlier observations of rapid magnetic field changes [*Phan et al.*, 2007] and particle flows in simulations [*Shay et al.*, 2007; *Karimabadi et al.*, 2007] of symmetric reconnection. For asymmetric reconnection the situation is different because these flows should be from only one side of the X line and only for a nonzero guide field [*Pritchett and Mozer*, 2009a].

[12] 6. The ion outflow speed is small near the X line. In Figure 3b the ion outflow speed relative to the Alfven speed is plotted. It approaches one at the highest flow regions, but it is much less than one through most of the box surrounding the X line. In Figure 5a the ratio of the measured outflow speed to the Alfven speed is given over a longer time span because ion moments were only obtained at the 3 s spin period. Also shown, for context, is B_Z which was zero in the region of interest at t = 44 s in this plot. Because the ion outflow speed was less than 10% of the Alfven speed in Figure 5a at the time of interest, the experimental data strongly suggest that the spacecraft passed through the vicinity of the X line.

[13] 7. The electric field, **E**, differs from $-\mathbf{U}_I \times \mathbf{B}$, where U_I is the ion flow speed. This fact is illustrated for one component in the simulation of Figure 3c, in which $(\mathbf{E} + \mathbf{U}_I \times \mathbf{B})_Y \neq 0$ both at the X line but also through a much larger region. Comparison of the measured three components of **E** and $-\mathbf{U}_I \times \mathbf{B}$ are given in Figures 5b–5d, where it is seen that the two quantities differed by as much as 25 mV/m during the crossing.

[14] 8. The parallel electric field has a spiky structure in space. In Figure 3d the expected parallel electric field has a spiky structure in space such that it may or may not be seen during a single satellite pass. The measured parallel electric field is given in Figure 6 which shows the measured plasma density in Figure 6a and the electric and magnetic field components in Figures 6b–6g during the 0.7 s interval when B_Z was zero at the X line crossing. The magnetic field data came from the search coil magnetometer which does not have a DC response. The fields are plotted in a magnetic field-aligned coordinate system whose Z direction is parallel to the average local magnetic field and are denoted by small letters to distinguish these fields from those in the minimum variance coordinate system. The measured parallel electric field in Figure 6d was zero to within the ~5 mV/m measurement uncertainty except during a 4 ms duration, 15 mV/m pulse at about 0.64 s. If this pulse crossed the spacecraft at any speed less than hundreds of km/s, the electric potential associated with it was less than a few tens of volts. Thus, the parallel electric field observed near the X line was both consistent with expectations from simulations and unimportant for accelerating the electron jet to several keV. The observed spiky field is also consistent with earlier measurements of parallel electric fields [*Mozer and Pritchett*, 2010] in terms of their amplitude, spiky nature, and occurrence frequency.

[15] It is noted that the several keV electron flux could, in principle, have been due to a brief enhancement of the perpendicular electron temperature by a factor greater than 20. This possibility has been compared with the jet hypothesis

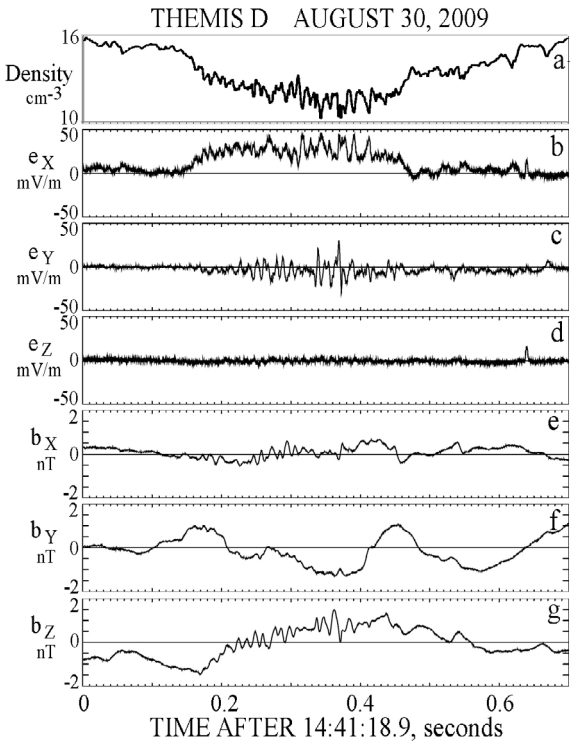

Figure 6. Waves observed in the plasma density, electric field, and magnetic field during a 0.7 s interval at or near the X line. The data are in magnetic field-aligned coordinates.

and the stronger, but inconclusive evidence is that these electrons formed a beam and not a temperature enhancement. The arguments include:

[16] 1. Simulations [*Karimabadi et al.*, 2007; *Shay et al.*, 2007; *Pritchett and Mozer*, 2009a] and experimental data [*Phan et al.*, 2007] have shown that a super-Alfvenic electron beam is generated at the X line.

[17] 2. A greatly enhanced perpendicular electron temperature at the X line has not been observed in simulations.

[18] 3. The electron pitch angle distribution of 90 ± 10 degrees, the energy spectrum, and the large temperature enhancement are difficult to understand in terms of perpendicular heating. Waves that can produce such heating were not observed.

[19] 4. Magnetic field variations with magnitudes and temporal variations similar to those expected from a current jet are present at the time of the enhanced energetic electrons and at other times. It is not possible to separate such magnetic field variations into those associated with a current and those associated with an erratic spacecraft trajectory through a spatially or time varying magnetic field. Thus the magnetic field data are consistent with, but do not prove, the existence of a current jet.

[20] 5. The short duration of the electron flux combined with changes of the magnetic field direction and limitations of the angular coverage of the data make it impossible to separate the effects of spatial and temporal variations of a hot perpendicular component from those due to a directed beam.

[21] 6. The 3 s determinations of the electron moments from plasma measurements include contributions from the dominant low-energy electrons, so they do not reveal significant information about the more rapid variations of the energetic electrons.

[22] It is noted that the observation of the largest flux of 1 keV electrons in 900 orbits across the dayside magnetopause is significant for understanding reconnection regardless of whether those electrons were a beam, as assumed in the present analysis, or a perpendicular temperature enhancement.

3. Waves and Their Effects

[23] To discuss the anomalous drag associated with the waves in the electric field components shown in Figures 2e, 2f, and 2h, as well as the waves in Figure 6, the anomalous drag term, $D_Y \equiv -\langle \delta n \delta E_Y \rangle / \langle n \rangle$ is utilized [*Drake et al.*, 2003; *Che et al.*, 2011; *Mozer et al.*, 2011]. In this equation, δn and δE_Y are the fluctuating components of the density, n, and the electric field component, respectively, and the drag depends on the average correlation of these fluctuations. This term arises from the average of Newton's second law by considering that $n = [\langle n \rangle + \delta n]$ and $E_Y = [\langle E_Y \rangle + \delta E_Y]$. Thus, the electric field force term $enE_Y = [e\langle n \rangle \langle E_Y \rangle + e\delta n \delta E_Y + e\langle E_Y \rangle \delta n + e\langle n \rangle \delta E_Y]$. After averaging this expression over several oscillations of the fluctuating components, one obtains the above expression for the anomalous drag that is evaluated for the case at hand. The average in the equation is over space [*Drake et al.*, 2003] while the data are averaged over time. Because of the rapid motion of the structures with respect to the spacecraft these two averages are assumed to be equivalent. (It is noted that the anomalous drag is sometimes estimated as due to an anomalous resistivity that is said to be proportional to the current density. This ad hoc formalism is replaced by the anomalous drag described above.)

[24] The large amplitude electric field waves of Figure 2 occurred mainly outside the magnetospheric separatrix. The wavelet spectrum of the turbulence in E_Y is shown in Figure 2g, in which the red line is the lower hybrid frequency. This turbulence is associated with the electrostatic lower hybrid drift instability arising in the plasma density gradient of Figure 2d. D_Y during this turbulence was correlated with the 5–15 mV/m E_Y but it contributed less than 10% of E_Y (not shown), in agreement with earlier work [*Mozer et al.*, 2011]. In the current layer, D_Y was less than 1% of E_Y, as is suggested by the absence of wave activity in Figure 2g through the current layer.

[25] During the 0.2 s wave event near the X line in Figure 6, the plasma density in Figure 6a and e_X in Figure 6b were anticorrelated (correlation coefficient = −0.94) while b_Z of Figure 6g was correlated with e_Y of Figure 6c (correlation coefficient after phase shift = 0.72). Thus the 0.2 s wave interval at the X line involved both electrostatic and electromagnetic waves whose frequencies were close to the lower hybrid frequency. The anticorrelation of density and e_X suggests that D_X during this 0.2 s time interval might be important. However, as shown in Figure 7, the 0.1 s average of the drag, while correlated with the 0.1 s averaged e_X, had an amplitude that was less than about 1% of e_X (note that the plotted quantity is $10*D_X$). Thus, anomalous drag due to

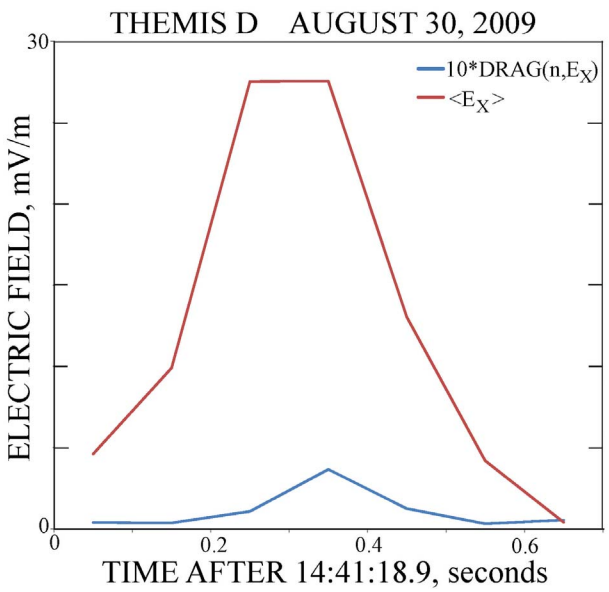

Figure 7. The 0.1 s averaged electric field and anomalous drag, D, during the 0.7 s time interval of interest.

the electrostatic wave component was not sufficient to account for the electric field or the dissipation required to accelerate the electron jet. The 30–60 Hz waveforms (lower hybrid frequency equaled 34–40 Hz) for e_Y and b_Z during this 0.4 s interval are plotted in Figure 8, in which it is seen that they are 90° out of phase and the ratio of e_Y to b_Z is 24 mV/m-nT. Because of the phase shift, these waves carry little net Poynting flux so they are not associated with the energy required for acceleration of the energetic electron jet. To conclude, the properties of this wave mode are:

[26] 1. The wave frequency was about equal to the lower hybrid frequency.

[27] 2. The magnetic field fluctuations were dominantly parallel to the background magnetic field.

[28] 3. The electric and magnetic field components were 90° out of phase.

[29] 4. The ratio of e_Y to b_Z was 24 mV/m-nT.

4. Dispersion Analysis

[30] This wave mode will next be considered via a linear kinetic Vlasov-Maxwell theory which assumes that, at the bifurcation point at the center of the current sheet, the plasma is locally homogeneous. In a homogenous plasma, waves with frequencies around and close to f_{LH} (where f_{LH} is the lower hybrid frequency) belong to the lower-hybrid plateau, which is electrostatic for strictly perpendicular k vectors, but electromagnetic for oblique angles. For very large $k_\perp$, this wave mode goes over into negatively dispersed Bernstein waves. For longer wavelengths (smaller k) the lower-hybrid plateau goes over into the right-hand polarized whistler mode. For frequencies above f_{LH} and below the electron cyclotron frequency, f_{ce}, this is the electron whistler mode. For frequencies $f_{cp} < f < f_{LH}$, it is often called the proton whistler mode, since the ion inertia becomes increasingly more important at lower frequencies and longer wavelengths. This mode, being essentially the same branch as the electron whistler, is also right-hand polarized with respect to the background magnetic field, B_o. In the long-wavelength limit, this branch can be viewed as the extension of the MHD fast mode.

[31] The program WHAMP [*Roennmark*, 1982] is used to calculate the wave dispersion and polarization properties. The plasma model is determined from the observations as $n = 11.5/cm^3$, $B_o = 61$ nT, $T_i = 0.7$ keV, $T_e = 0.09$ keV, $T_{perp}/T_{par} = 1$ for both species, and it consists of stable Maxwellians. Thus the analysis does not address the instability creating the waves, but only the damping $\gamma/f_{cp} < 0$, where γ is the imaginary part of the frequency. The analysis thus shows which modes are permissible with the given plasma parameters.

[32] Figure 9 shows the lower-hybrid (LH) plateau for $10^{1.2} < k_\perp \rho_p < 10^2$ and $10^{-7} < k_\parallel \rho_p < 10^{-2}$, where ρ_p is the proton gyroradius. The frequency is normalized to the proton gyrofrequency, f_{cp}. The waves have a very small damping rate for perpendicular wave vectors and are only slightly more damped for oblique angles, as shown by the color bar. For smaller perpendicular wave numbers, $k_\perp$, the damping rate increases and the waves eventually become so heavily damped close to the intersection with the whistler branch that no mode conversion at, for example, density gradients, seems plausible (not shown). Waves generated on the LH plateau therefore are likely to stay in that mode. The right-hand whistler branch is permissible (low damping rate) for lower frequencies, but since it is not observed, it is not analyzed further.

[33] The numerical analysis shows that the parallel wave magnetic field and the perpendicular wave electric field are exactly 90 degrees out of phase on the LH plateau of Figure 9, in perfect agreement with the satellite observations of Figure 8.

[34] The wavelength of the waves may be deduced by comparing the observed ratio, $de_Y/db_Z = 24$ mV/m-nT, with the theoretical value calculated from the kinetic model. This experimental value corresponds to the model $k_\perp \rho_p \sim 10^{1.65}$, which gives a wavelength $\lambda \sim \lambda_\perp \sim 9$ km. The waves thus have a wavelength the order of the electron skin

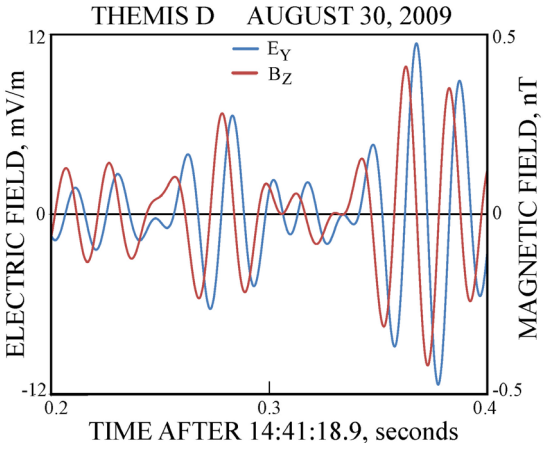

Figure 8. Electric and magnetic field waveforms in an electromagnetic wave whose E and B fields were 90° out of phase.

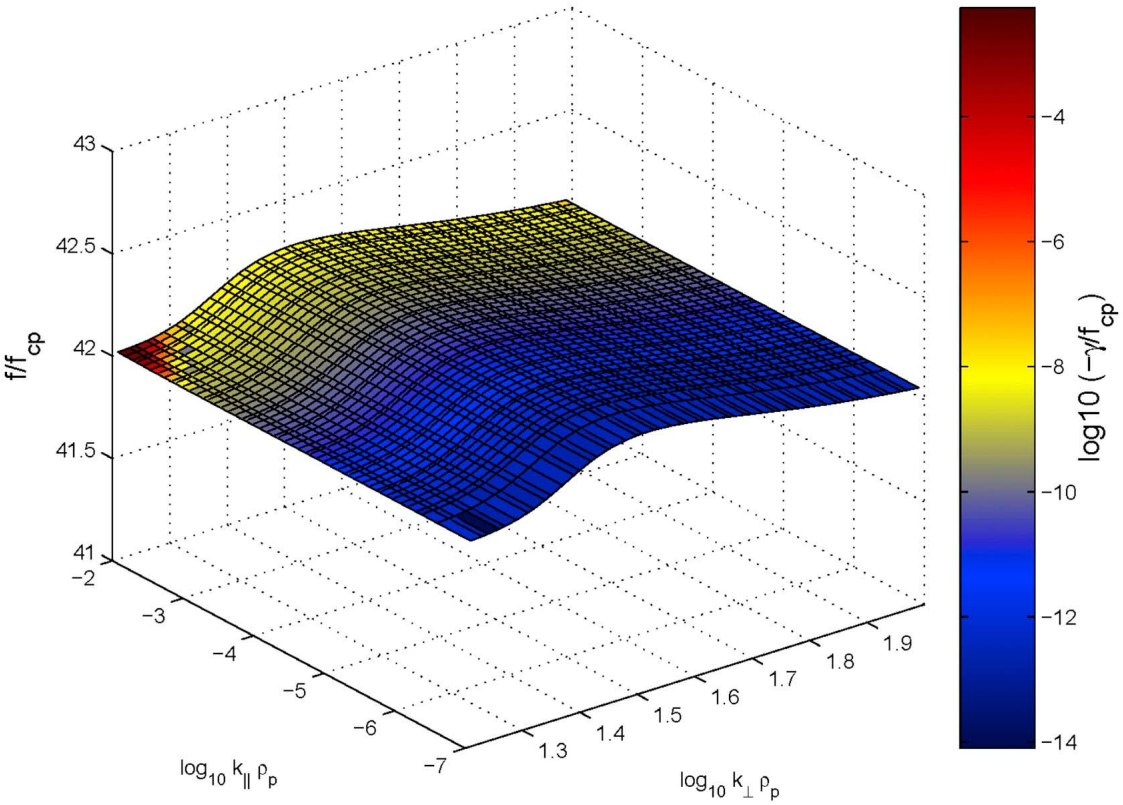

Figure 9. Lower hybrid plateau from a numerical Vlasov-Maxwell calculation.

depth ($\lambda_e \sim 2$ km), as expected near the X line [*Pritchett and Mozer*, 2009b].

[35] Note that the wave surface is localized around f_{LH} but it has a slightly distorted shape which allows for a small group velocity in the perpendicular direction for wave numbers around $k_\perp \rho_p \sim 1.35$. This low group speed is consistent with the wave electric and magnetic fields being 90° out of phase, as in Figure 8, which results in a negligible Poynting flux. The parallel group velocity is very close to zero.

5. Conclusions

[36] 1. A satellite crossing has been identified as occurring near the reconnection X line from measurements of the plasmas, fields and waves at the crossing.

[37] 2. An accelerated electron jet was observed to flow perpendicular to the magnetic field near the X line at a speed that was more than an order of magnitude greater than the $(\mathbf{E} \times \mathbf{B}/B^2)_Z$ computed from direct measurements and a few times the local electron Alfven speed discussed above.

[38] 3. An electromagnetic wave was measured close to the X line and its properties agree with those obtained from a dispersion analysis which showed: (1) the waves were on the lower hybrid branch; (2) the electric and magnetic fields were 90° out of phases and they carried almost no Poynting flux; (3) the wave magnetic field was parallel to the local background magnetic field; and (4) the wavelength of the electromagnetic wave was inferred to be 9 km, which is a few times the electron skin depth.

[39] 4. An electrostatic wave was measured near the X line and the correlations between its density and electric field fluctuations produced an anomalous drag that was too small to support the observed low-frequency electric field.

[40] 5. The electrostatic and electromagnetic waves as well as the low-frequency electric field were not sufficient to account for the acceleration of the super-Alfvenic electrons if that acceleration occurred over a distance of a few electron skin depths. Possible explanations of this acceleration are that it occurred over much larger distances or that fields at some other locale provided the acceleration.

[41] 6. Because the anomalous drag due to the electrostatic wave at the X line was insufficient to support the observed electric field, the remaining terms in Newton's second law must be responsible for this field. The 30% plasma density change of Figure 6a suggests the possibility that the divergence of the pressure tensor could be important because the density gradient over an electron skin depth associated with this change is equivalent to an electric field of tens of mV/m.

[42] The measurements near the X line for this crossing, showing no large parallel or perpendicular electric fields and little wave turbulence, anomalous drag or Poynting flux, agree with earlier simulations [*Pritchett and Mozer*, 2009b] and with a second, similar crossing of THEMIS D on 26 September 2010 just after 19:33 UT.

[43] **Acknowledgments.** This work was supported by NASA grants NNX09AE41G-1/11 and NNX11AD74G and by NASA contract NAS5-02099-09/12. The computations in this work were made possible by allocations of advanced computing resources provided by the National Science Foundation on Kraken (a Cray XT5) at the National Institute for Computational Sciences (http://www.nics.tennessee.edu) and by the NASA

High-End Computing Program through the NASA Advanced Supercomputing Division at Ames Research Center.

[44] The Editor would like to thank James Birch and the other reviewers for their assistance in evaluating this paper.

References

Che, H., J. F. Drake, and M. Swisdak (2011), A current filamentation mechanism for breaking magnetic field lines during reconnection, *Nature*, *474*, 184–187, doi:10.1038/nature10091.

Drake, J. F., M. Swisdak, C. Cattell, M. A. Shay, B. N. Rogers, and A. Zeiler (2003), Formation of electron holes and particle energization during magnetic reconnection, *Science*, *299*, 873–877, doi:10.1126/science.1080333.

Karimabadi, H., W. Daughton, and J. Scudder (2007), Multi-scale structure of the electron diffusion region, *Geophys. Res. Lett.*, *34*, L13104, doi:10.1029/2007GL030306.

Mozer, F. S., and P. L. Pritchett (2010), Spatial, temporal, and amplitude characteristics of parallel electric fields associated with subsolar magnetic field reconnection, *J. Geophys. Res.*, *115*, A04220, doi:10.1029/2009JA014718.

Mozer, F. S., M. Wilber, and J. F. Drake (2011), Wave associated anomalous drag during magnetic field reconnection, *Phys. Plasmas*, *18*, 102902, doi:10.1063/1.3647508.

Phan, T. D., J. F. Drake, M. A. Shay, F. S. Mozer, and J. P. Eastwood (2007), Evidence for an elongated (>60 ion skin depths) electron diffusion region during fast reconnection, *Phys. Rev. Lett.*, *99*, 255002, doi:10.1103/PhysRevLett.99.255002.

Pritchett, P. L., and F. S. Mozer (2009a), Asymmetric magnetic reconnection in the presence of a guide field, *J. Geophys. Res.*, *114*, A11210, doi:10.1029/2009JA014343.

Pritchett, P. L., and F. S. Mozer (2009b), The magnetic field reconnection site and dissipation region, *Phys. Plasmas*, *16*, 080702, doi:10.1063/1.3206947.

Roennmark, K. (1982), Waves in Homogeneous, Anisotropic Multicomponent Plasmas (WHAMP), *Rep. 179*, Kiruna Geofys. Inst., Kiruna, Sweden.

Shay, M. A., J. F. Drake, and M. Swisdak (2007), Two-scale structure of the electron dissipation region during collisionless magnetic reconnection, *Phys. Rev. Lett.*, *99*, 155002, doi:10.1103/PhysRevLett.99.155002.

Swisdak, M., J. F. Drake, M. A. Shay, and J. G. McIlhargey (2005), Transition from antiparallel to component magnetic reconnection, *J. Geophys. Res.*, *110*, A05210, doi:10.1029/2004JA010748.

J. P. McFadden, F. S. Mozer, I. Roth, and D. Sundkvist, Space Sciences Laboratory, University of California, Berkeley, CA 94720, USA. (fmozer@ssl.berkeley.edu)

P. L. Pritchett, Department of Physics and Astronomy, University of California, Los Angeles, CA 90095, USA.